VCST Internal Memo

Title: Estimate of Radiometric Uncertainty for the S-NPP Thermal Bands On-orbit
Memo Number: 2013_002
Revision: 01
Date: September 5, 2013
Author: Jeff McIntire and Boryana Efremova
To: Xiaoxiong Xiong and James Butler
Cc: Hassan Oudrari, Kwo-Fu (Vincent) Chiang, Jon Fulbright and Aisheng Wu

References

[1] An Introduction to Error Analysis, John R. Taylor, University Science Books, 1997.
[2] NICST_MEMO_11_014, 'Uncertainty Estimate for the Thermal Band Radiometric Retrievals,' Jeff McIntire, October 5, 2011.
[3] NICST_MEMO_11_001, 'Analysis of the Radiometric Calibration from VIIRS F1 RC-05 Part 1 Test (Nominal Plateau, Electronic Side B),' Jeff McIntire and Sanxiong Xiong, January 3, 2011.
[4] 'Performance Verification Report – VIIRS FU1 Emissive Band Calibration (PVP Section 4.2.4),' Karen Galang, December 4, 2009, revision E.
[5] PL3095-N06593, 'Absolute Radiometric Calibration Thermal Region: Uncertainty Estimates,' Jim Young, 1997.
[6] NICST_MEMO_08_008, 'Response vs. Scan Angle for VIIRS FU1 TEB (FP-10, part 2),' Sanxiong Xiong, Chunhui Pan, and Nianzeng Che, March 11, 2008.
[7] VCST_TECH_MEMO_2012_029, 'Calibrating NPP VIIRS M13LG fire detection band by comparing M13LG and M13HG images of the Moon in the Space View,' Boryana Efremova and Jeff McIntire, December 3, 2012.
[8] 'NPP Visible/infrared Imager Radiometer Suite (VIIRS) Radiance Uncertainty, Emissive Bands – Tested Performance', E. Johnson, K. Galang, C. Ranshaw, and B. Robinson, *Proc of SPIE* 7808, 78081F (2010).

1. Introduction

VIIRS thermal band SDR products (TOA radiance and brightness temperature) are used in a number of different science products. It is important to estimate the uncertainty of these measurements for science team evaluations of the down stream products. This work will focus on propagating the uncertainty inherent in the S-NPP VIIRS TEB measurements to the SDR product level. The uncertainty is propagated using the standard formulation [1], as is described in the following section. Results of the error propagation are investigated for different Earth scene temperatures and conditions (scan angle and aggregation mode). The estimates contained in this work are compared to the uncertainties derived at the time of sensor level TV testing [2].

2. Error Propagation

For the purposes of this work, we follow the standard propagation of error for a function y of variables x_i is described by [1]

$$u^2(y) = \sum_{i=1}^{N} \left(\frac{\partial y}{\partial x_i} \right)^2 u^2(x_i) + 2 \sum_{i=1}^{N-1} \sum_{j=i+1}^{N} \left(\frac{\partial y}{\partial x_i} \right) \left(\frac{\partial y}{\partial x_j} \right) u(x_i, x_j). \qquad (1)$$

Here $u(x_i)$ is the uncertainty of the variable x_i that goes into the calculation of the y and $u(x_i,x_j)$ is the covariance between x_i and x_j. The Earth View (EV) retrieved radiance was defined in [3] and is a function of

$$L_{ret}^{EV} = f(c_0, c_1, c_2, L_{BB}, L_{HAM}, L_{RTA}, L_{CAV}, L_{SH}, F_{SH}, F_{CAV}, F_{RTA}, RVS_{BB}, RVS_{EV}, RVS_{SV}, \varepsilon_{BB}, \rho_{RTA}, dn_{EV}, dn_{BB}) . \quad (2)$$

The partial derivatives for each variable are listed in Appendix A for the Blackbody (BB) path difference radiance and Appendix B for the EV retrieved radiance. Note that the total uncertainty here is for a single EV pixel; the effects of aggregation and scan angle will also be investigated in Section 4.

In general, the covariance terms were not directly calculated (the exception is the covariance terms between the radiometric coefficients); a direct calculation of these terms is beyond the scope of this work. However, an upper bound on the covariance terms is determined through use of the Schwarz inequality [1], or

$$\left|u(x_i, x_j)\right| \le u(x_i)u(x_j) \quad (3)$$

Results will be presented without covariance terms (excepting those terms between the radiometric coefficients) as a baseline and with covariance terms determined using the Schwarz inequality as a worst case estimate.

3. Individual Error Sources

In this section we describe the individual uncertainty contributors. The descriptions follow from [3] with some additions unique to on-orbit operations.

3.1 Radiances

The radiance uncertainty for each of the radiances that factor into the present calculation (L_{BB}, L_{HAM}, L_{RTA}, L_{SH}, and L_{CAV}) is the RSS of the uncertainty contributors. Each of these radiances was converted from a temperature reading provided by one or more thermistors once per scan using the Planck equation, integrated over the spectral response of the instrument. In the cases where more than one thermistor was used, the average was employed in the Planck equation. The error is composed of four components: temperature, spectral, interpolation, and statistical uncertainty.

The temperature uncertainties used in this analysis are listed in Table 1 [4]. The radiance uncertainty associated with temperature error was determined by taking the absolute value of the maximum difference between the Planck radiance at a given temperature and at the ends of the temperature uncertainty interval, or

$$u(L) = \max\left(\left|L(T,\lambda) - L(T \pm \Delta T, \lambda)\right|\right). \quad (4)$$

The spectral errors used here are listed in Table 2 [5]. The radiance uncertainties due to spectral errors were determined in the same manner as the temperature uncertainties,

$$u(L) = \max\left(\left|L(T,\lambda) - L(T, \lambda \pm \Delta\lambda)\right|\right). \quad (5)$$

On-orbit, the calibration relies on LUTs to convert source temperature to radiance. A linear interpolation is used to determine the radiance at the actual source temperature every scan. The interpolation uncertainty is determined by the following,

$$u(L) = \frac{1}{2}(T - T_0)(T - T_1) f^{(2)}(T) \quad (6)$$

where T_0 and T_1 are the LUT values bracketing the measured T and the second derivative is of Planck's radiation law with respect to the measured T.

The statistical uncertainties were the standard deviation of the radiances determined within one granule (or over 48 scans).

3.2 Response Versus Scan (RVS)

The uncertainties for the RVS factors were determined in [6]. The on-orbit RVS was normalized relative to the solar diffuser HAM angle. The RVS uncertainty derived from FP-10 was a combination of fitting error and measurement error [6]; the band averaged values used in this work are given in Table 3 (where the average of the M16A and M16B uncertainties was used for M16). Any scan angle dependence to the uncertainty was not considered. No uncertainty due to emission versus scan was included in the present work.

3.3 BB Reflectance Shape Factors, Reflectance of the RTA, and Emissivity of the BB

The uncertainties for the BB reflectance shape factors are all taken to be 100%. The uncertainty for the reflectance of the RTA is 0.5% at 270 K [4]. This uncertainty was used for all source temperature levels. The BB emissivity was measured at 3.39 μm; the error in the emissivity measurement was determined to be 0.07% [4]. This uncertainty was used for all thermal bands.

3.4 EV and BB Response

The uncertainty in the response was the RSS of the precision and accuracy errors for the background subtracted digital response. The precision error was the standard deviation over all analyzed samples and scans; for the purposes of this work:

- The precision error for the single EV pixel cannot be calculated directly. A fit of standard deviations over the BB view samples derived during the BB WUCD from 12/2012 was used to estimate the precision error in a given EV pixel as a function of detector signal.
- The precision error for the BB view is the standard deviation of the mean over the 48 samples per scan and 48 scans in a granule

The accuracy error was the RSS of the known biases. Any bias common to all sectors would be removed in the background subtraction. The known biases between sectors are listed below [4]:

- The EV response was reported in a truncated 12 bit format, whereas the calibration sectors were reported in 14 bits; this creates a bias of about 0.375 dn in the SV relative to the EV. To compensate, all calibration view data can be truncated to 12 bits at the beginning of the processing. The bias is then common to both sectors and is eliminated in the background subtraction.
- There is an additional bias in the EV data due to aggregation. In a three pixel aggregation zone, each pixel is truncated to 12 bits. Then the three pixels are averaged, and the average is truncated to 12 bits. A similar process was used for the two pixel aggregation zone. To compensate in the analysis, all calibration view data can be processed in a manner similar to the EV data. The bias is then common to both sectors and is eliminated in the background subtraction.

- For M13, there is a small bias between fixed and auto gain configurations (a few tenths of a DN). Currently, the cause has not been determined [4]. This bias was not included in the present analysis.
- There is also a bias in the EV data for M16 TDI. Each M16A and M16B detector response is first truncated to 12 bits. Then the average of the two detector responses is taken, and that average is again truncated to 12 bits. To compensate in the analysis, all calibration view data can be processed in a manner similar to the EV data. The bias is then common to both sectors and is eliminated in the background subtraction.

As this analysis was conducted at model dn values (as described below), all the precision errors that can be removed via processing were not included in this analysis. The exception is the M13 bias between auto and fixed gain modes; as this bias is not currently understood, it was not included in this analysis.

3.5 Radiometric Coefficients

The vertical least-squares fitting algorithm used in this memo determined the vertical deviations of the set of data points from the fit, or

$$R^2 = \sum \left[\Delta L_i - c_0 - c_1 dn_i - c_2 dn_i^2\right]^2 . \quad (7)$$

The minimum of the vertical deviations was computed by setting the partial derivatives with respect to coefficients equal to zero, or

$$\frac{\partial R^2}{\partial c_i} = 0 . \quad (8)$$

This led to the following matrix equation:

$$\begin{bmatrix} c_0 \\ c_1 \\ c_2 \end{bmatrix} = \begin{bmatrix} N & \sum dn & \sum dn^2 \\ \sum dn & \sum dn^2 & \sum dn^3 \\ \sum dn^2 & \sum dn^3 & \sum dn^4 \end{bmatrix}^{-1} \begin{bmatrix} \sum \Delta L \\ \sum dn\, \Delta L \\ \sum dn^2 \Delta L \end{bmatrix}, \quad (9)$$

where N is the number of points used in the fit and we define

$$A = \begin{bmatrix} N & \sum dn & \sum dn^2 \\ \sum dn & \sum dn^2 & \sum dn^3 \\ \sum dn^2 & \sum dn^3 & \sum dn^4 \end{bmatrix}^{-1} . \quad (10)$$

The solution to this matrix equation determined the radiometric coefficients determined from the periodic BB warm-up cool-down (WUCD) cycles. This algorithm also produced 1-sigma uncertainties and covariance terms. The variance of the fitting points with respect to the fit was determined by

$$\sigma_{fit}^2 = \frac{1}{N-3} \sum_{i=1}^{N} \left(\Delta L_i - c_0 - c_1 dn_i - c_2 dn_i^2\right)^2 , \quad (11)$$

which is an indicator of the error in the measurements. The coefficient uncertainties and covariance terms are defined by the following:

$$u(c_i) = \sigma_{fit}^2 \sqrt{A(i,i)} , \quad (12)$$

$$u(c_i, c_j) = \sigma_{fit}^2 A(i,j) . \quad (13)$$

This approach assumes that the uncertainties in ΔL are roughly constant over the data points used (and the uncertainties in dn are negligible). However, this algorithm only included some effects from precision error (random statistical variations), but excluded any bias uncertainties (accuracy error). Furthermore, it should be noted that the uncertainties are valid only insomuch as the model itself is valid. The quality of the radiometric fitting for the thermal bands has been discussed in previous work

[2]. For the purposes of this memo, the radiometric model is considered sufficiently valid to proceed with the uncertainty analysis.

4. Analysis

The uncertainty propagation was performed for each band at a series of model dn levels (5, 20, 100, 250, 500, 750, 1000, 1500, 2000, 2500, 3000, and 3500). The radiometric coefficients used in this work were derived from the 12/2012 WUCD so that the uncertainties would be traceable (uncertainties for the operational SDR coefficients were not provided).

The exception is M13 low gain, where uncertainties roughly the difference from derived on-orbit coefficients from lunar analysis [7] for the operational coefficients are used in conjunction with the operation coefficients. The lunar analysis derived coefficients are in general agreement with the coefficients derived in [3]. As the offset is consistent with zero, an uncertainty of 100% is used for the operation offset uncertainty. An uncertainty of about 7.4% is used for the operational linear coefficient. The nonlinear term is neglected (its contribution is negligible and cannot be derived on-orbit).

Aggregation zone and scan angle effects were also investigated. The aggregation zone influence was estimated by including an additional factor of $1/\sqrt{2}$ or $1/\sqrt{3}$ in the EV dn uncertainty. The scan angle effects were investigated by determining the uncertainty at scan angles -54.2, -35.4, 0.0, 35.4, and 54.2.

In [2], it was postulated that propagating the uncertainty at the retrieved radiance level includes some double counting, as the errors in the source path difference radiance are propagated into the fitting coefficient uncertainties as well as contribute at the retrieved radiance level. In that work, the uncertainties in the BB path difference radiance were propagated into the coefficients errors using the random measurement error, and not included at the product level error propagation. In the current work, the uncertainties present in the BB path difference radiance were also included at the product level error propagation; however, the overall uncertainty was not significantly affected.

5. Results

Figures 1 – 7 plot the individual uncertainty contributors in % of the retrieved radiance for each band (detector 9, HAM side A) as a function of scene temperature. For the MWIR, the BB radiance term is the most important at higher temperatures and the EV dn term dominates at lower temperatures, increasing rapidly as the temperature decreases (note the BB is nominally controlled at ~ 292 K). The c_2 term also becomes important at the highest temperatures. In the LWIR, no terms are particularly dominant at higher temperatures, while the EV dn and c_0 terms predominate at the lowest scene temperatures (again increasing rapidly). The RVS terms also become important at lower temperatures for the LWIR. The case of M13 LG shows that the largest terms are the radiometric coefficients (c_0 at lower temperature and c_1 at higher temperatures).

The total uncertainties per band for detector 9, HAM side A are shown in Figure 8 (in % of radiance) and Figure 9 (in K) versus scene temperature. All bands exhibit roughly constant uncertainty at higher scene temperatures. In Figure 8, the bands show less than ~1 % radiance uncertainty above scene temperatures ~280 K (I4), ~260 K (M12 and M13), ~230 K (I5 and M14), and ~210 K (M15 and M16). In terms of temperature uncertainty, all bands show less that ~0.5 K above scene temperatures ~260 K (I4), ~ 240 K (M12 and M13), ~230 K (I5), and ~210 K (M14, M15, and M16). The total radiance uncertainties for M13 LG in %, and temperature uncertainties in K are shown in Figures 10 and 11, respectively. The radiance uncertainty is roughly constant at ~7.5 % at higher scene temperatures (due

mainly to c_1) and rises below 400 K to roughly 25 % (largely as the result of c_0); in terms of temperature uncertainty, M13 LG exhibits uncertainties of about 8 K near the 350 K, decreasing to about 4 K between 400 and 450 K, and then increasing slowly to about 8 K at scene temperatures of 650 K.

The total uncertainties are compared to the specifications in Tables 4 and 5 (in terms of % of radiance and temperature [K], respectively) for all bands, detector 9, HAM side A. There are some non-compliances at lower scene temperatures for bands M12, M13, M15, and M16; however, in all cases, the non-compliances are small (within 0.13 K). It should be noted that pre-launch analysis showed these bands to be compliant (but in general only marginally for the non-compliances reported here) [2,8]. The differences from pre-launch uncertainty estimates are largely attributed to the estimation of the EV dn uncertainty. Pre-launch this term was estimated from an extended, external source over many scans; post-launch, the uncertainty was determined from on-board BB warm-up cool-down data as described in section 3.4. As the lowest measured temperature for the on-board BB is ~267 K, there is some additional uncertainty in estimating the EV dn uncertainty for lower scenes.

The variation with scan angle (and aggregation mode) was also calculated as seen in Figures 13 – 19 for all bands (detector 9, HAM side A shown). Note that the specification is shown with a dashed red line. The MWIR bands show dependence on aggregation zone, where the interior aggregation zones have lower uncertainty. This is the result of the lower uncertainty in the EV dn contribution (included here as the decrease in uncertainty associated with averaging 2 or 3 pixels: $1/\sqrt{2}$ or $1/\sqrt{3}$). In M14, the uncertainty exhibits a dependence on scan angle, where lower uncertainty is observed at beginning of scan. This is the result of the RVS difference from the EV and space view paths. This difference increases from beginning of scan to end of scan. The other LWIR bands do not show much variation (some small scan angle dependence).

Figures 20 and 21 show the total uncertainties for both the baseline and worst-case approaches. The worst-case uncertainties are always larger than the baseline, with the smallest difference at ~292 K. Below this temperature, the worst-case uncertainty is about 0.2 K larger. Above 292 K, the differences increase to about 0.3 K at scene temperatures of 350 K. The worst-case uncertainty likely represents an overestimate as covariance terms must be smaller that the Schwarz inequality and may even be negative.

6. Summary

Uncertainty estimates for the thermal band radiometry retrievals were determined by propagating the error estimates from the individual uncertainty sources. This uncertainty model was applied to the case of a single EV pixel. The following is a list of findings:

- Total uncertainties for each band were compared to specified uncertainty limits at a series of scene temperatures. For most cases, the estimated uncertainties were below the limits. However, some lower scene temperatures showed uncertainties above the specification.
- In general, the modeled uncertainty estimates were in good agreement with pre-launch estimates. Some lower scene temperatures had slightly higher uncertainties, resulting in non-compliances with the specification that were absent in the pre-launch calculation.
- MWIR EV retrieved radiance uncertainties are between 0.2 – 0.3 K at high scene temperatures and increase rapidly below 250 K for M12 and M13 and 270 K for I4. LWIR EV retrieved

radiance uncertainties are between 0.2 – 0.4 K above scene temperatures of between 210 – 230 K.

- Dominant terms in MWIR EV uncertainties are BB radiance error (roughly constant with scene temperature) and EV dn uncertainties (increasing rapidly with decreasing scene temperature). No term was dominant in the LWIR EV uncertainties at higher scene temperatures whiles c_0, RVS, and EV dn uncertainties all increased at lower scene temperatures.
- MWIR band uncertainties showed decreased uncertainty at lower scene temperatures for the interior aggregation zones. M14 uncertainties showed some dependence with scan angle at lower scene temperatures.
- M13 LG uncertainties estimated to be between 4 and 8 K; the uncertainties were dominated by the c0 and c1 terms (lower and higher scene temperatures respectively).

Appendix A

The following are the partial derivatives of the BB view path difference radiance with respect to the various contributors:

$$\frac{\partial \Delta L_{BB}}{\partial RVS_{BB}} = \varepsilon_{BB} L_{BB} + (1-\varepsilon_{BB})(F_{SH} L_{SH} + F_{CAV} L_{CAV} + F_{RTA} L_{RTA}) - \frac{1}{\rho_{RTA}}[L_{HAM} - (1-\rho_{RTA}) L_{RTA}]$$

$$\frac{\partial \Delta L_{BB}}{\partial RVS_{SV}} = \frac{1}{\rho_{RTA}}[L_{HAM} - (1-\rho_{RTA}) L_{RTA}]$$

$$\frac{\partial \Delta L_{BB}}{\partial L_{BB}} = RVS_{BB} \varepsilon_{BB}$$

$$\frac{\partial \Delta L_{BB}}{\partial L_{HAM}} = \frac{(RVS_{SV} - RVS_{BB})}{\rho_{RTA}}$$

$$\frac{\partial \Delta L_{BB}}{\partial L_{RTA}} = RVS_{BB}(1-\varepsilon_{BB}) F_{RTA} - \frac{(RVS_{SV} - RVS_{BB})}{\rho_{RTA}}(1-\rho_{RTA})$$

$$\frac{\partial \Delta L_{BB}}{\partial \varepsilon_{BB}} = RVS_{BB} L_{BB} - RVS_{BB}(F_{SH} L_{SH} + F_{CAV} L_{CAV} + F_{RTA} L_{RTA})$$

$$\frac{\partial \Delta L_{BB}}{\partial \rho_{RTA}} = -\frac{(RVS_{SV} - RVS_{BB})}{\rho_{RTA}^2}(L_{HAM} - L_{RTA})$$

$$\frac{\partial \Delta L_{BB}}{\partial F_{SH}} = RVS_{BB}(1-\varepsilon_{BB}) L_{SH}$$

$$\frac{\partial \Delta L_{BB}}{\partial F_{CAV}} = RVS_{BB}(1-\varepsilon_{BB}) L_{CAV}$$

$$\frac{\partial \Delta L_{BB}}{\partial F_{RTA}} = RVS_{BB}(1-\varepsilon_{BB}) L_{RTA}$$

$$\frac{\partial \Delta L_{BB}}{\partial L_{SH}} = RVS_{BB}(1-\varepsilon_{BB}) F_{SH}$$

$$\frac{\partial \Delta L_{BB}}{\partial L_{CAV}} = RVS_{BB}(1-\varepsilon_{BB}) F_{CAV}$$

Appendix B

The following are the partial derivatives of the retrieved EV radiance with respect to the various contributors:

$$\frac{\partial L_{ret}^{EV}}{\partial c_0} = \frac{\Delta L_{BB}}{RVS_{EV}} \frac{c_1\left(dn_{BB} - dn_{EV}\right) + c_2\left(dn_{BB}^2 - dn_{EV}^2\right)}{\left(c_0 + c_1 dn_{BB} + c_2 dn_{BB}^2\right)^2}$$

$$\frac{\partial L_{ret}^{EV}}{\partial c_1} = \frac{\Delta L_{BB}}{RVS_{EV}} \frac{c_0\left(dn_{EV} - dn_{BB}\right) + c_2\left(dn_{bB}^2 dn_{EV} - dn_{EV}^2 dn_{BB}\right)}{\left(c_0 + c_1 dn_{BB} + c_2 dn_{BB}^2\right)^2}$$

$$\frac{\partial L_{ret}^{EV}}{\partial c_2} = \frac{\Delta L_{BB}}{RVS_{EV}} \frac{c_0\left(dn_{EV}^2 - dn_{BB}^2\right) + c_1\left(dn_{EV}^2 dn_{BB} - dn_{BB}^2 dn_{EV}\right)}{\left(c_0 + c_1 dn_{BB} + c_2 dn_{BB}^2\right)^2}$$

$$\frac{\partial L_{ret}^{EV}}{\partial RVS_{BB}} = \left\{\varepsilon_{BB} L_{BB} + \left(1 - \varepsilon_{BB}\right)\left(F_{SH} L_{SH} + F_{CAV} L_{CAV} + F_{RTA} L_{RTA}\right) - \frac{1}{\rho_{RTA}}\left[L_{HAM} - \left(1 - \rho_{RTA}\right) L_{RTA}\right]\right\} \times \frac{\left(c_0 + c_1 dn_{EV} + c_2 dn_{EV}^2\right)}{RVS_{EV}\left(c_0 + c_1 dn_{BB} + c_2 dn_{BB}^2\right)}$$

$$\frac{\partial L_{ret}^{EV}}{\partial RVS_{EV}} = -\frac{\Delta L_{BB}\left(c_0 + c_1 dn_{EV} + c_2 dn_{EV}^2\right)}{RVS_{EV}^2\left(c_0 + c_1 dn_{BB} + c_2 dn_{BB}^2\right)} - \frac{RVS_{SV}}{\rho_{RTA} RVS_{EV}^2}\left[L_{HAM} - \left(1 - \rho_{RTA}\right) L_{RTA}\right]$$

$$\frac{\partial L_{ret}^{EV}}{\partial RVS_{SV}} = \frac{1}{\rho_{RTA}}\left[L_{HAM} - \left(1 - \rho_{RTA}\right) L_{RTA}\right]\left[1 + \frac{\left(c_0 + c_1 dn_{EV} + c_2 dn_{EV}^2\right)}{RVS_{EV}\left(c_0 + c_1 dn_{BB} + c_2 dn_{BB}^2\right)}\right]$$

$$\frac{\partial L_{ret}^{EV}}{\partial L_{RTA}} = \left[\left(1 - \varepsilon_{BB}\right) RVS_{BB} F_{RTA} - \frac{\left(RVS_{SV} - RVS_{BB}\right)}{\rho_{RTA}}\left(1 - \rho_{RTA}\right)\right] \frac{\left(c_0 + c_1 dn_{EV} + c_2 dn_{EV}^2\right)}{RVS_{EV}\left(c_0 + c_1 dn_{BB} + c_2 dn_{BB}^2\right)} - \frac{\left(RVS_{SV} - RVS_{EV}\right)}{RVS_{EV} \rho_{RTA}}\left(1 - \rho_{RTA}\right)$$

$$\frac{\partial L_{ret}^{EV}}{\partial L_{BB}} = \varepsilon_{BB} RVS_{BB} \frac{\left(c_0 + c_1 dn_{EV} + c_2 dn_{EV}^2\right)}{RVS_{EV}\left(c_0 + c_1 dn_{BB} + c_2 dn_{BB}^2\right)}$$

$$\frac{\partial L_{ret}^{EV}}{\partial L_{SH}} = \left(1 - \varepsilon_{BB}\right) RVS_{BB} F_{SH} \frac{\left(c_0 + c_1 dn_{EV} + c_2 dn_{EV}^2\right)}{RVS_{EV}\left(c_0 + c_1 dn_{BB} + c_2 dn_{BB}^2\right)}$$

$$\frac{\partial L_{ret}^{EV}}{\partial L_{CAV}} = \left(1 - \varepsilon_{BB}\right) RVS_{BB} F_{CAV} \frac{\left(c_0 + c_1 dn_{EV} + c_2 dn_{EV}^2\right)}{RVS_{EV}\left(c_0 + c_1 dn_{BB} + c_2 dn_{BB}^2\right)}$$

$$\frac{\partial L_{ret}^{EV}}{\partial L_{HAM}} = \frac{\left(RVS_{SV} - RVS_{BB}\right)}{\rho_{RTA}} \frac{\left(c_0 + c_1 dn_{EV} + c_2 dn_{EV}^2\right)}{RVS_{EV}\left(c_0 + c_1 dn_{BB} + c_2 dn_{BB}^2\right)} + \frac{\left(RVS_{SV} - RVS_{EV}\right)}{RVS_{EV} \rho_{RTA}}$$

$$\frac{\partial L_{ret}^{EV}}{\partial F_{SH}} = \left(1 - \varepsilon_{BB}\right) RVS_{BB} L_{SH} \frac{\left(c_0 + c_1 dn_{EV} + c_2 dn_{EV}^2\right)}{RVS_{EV}\left(c_0 + c_1 dn_{BB} + c_2 dn_{BB}^2\right)}$$

$$\frac{\partial L_{ret}^{EV}}{\partial F_{CAV}} = \left(1 - \varepsilon_{BB}\right) RVS_{BB} L_{CAV} \frac{\left(c_0 + c_1 dn_{EV} + c_2 dn_{EV}^2\right)}{RVS_{EV}\left(c_0 + c_1 dn_{BB} + c_2 dn_{BB}^2\right)}$$

$$\frac{\partial L_{ret}^{EV}}{\partial F_{RTA}} = \left(1 - \varepsilon_{BB}\right) RVS_{BB} L_{RTA} \frac{\left(c_0 + c_1 dn_{EV} + c_2 dn_{EV}^2\right)}{RVS_{EV}\left(c_0 + c_1 dn_{BB} + c_2 dn_{BB}^2\right)}$$

$$\frac{\partial L_{ret}^{EV}}{\partial \varepsilon_{BB}} = RVS_{BB}\left[L_{BB} + \left(F_{SH} L_{SH} + F_{CAV} L_{CAV} + F_{RTA} L_{RTA}\right)\right] \frac{\left(c_0 + c_1 dn_{EV} + c_2 dn_{EV}^2\right)}{RVS_{EV}\left(c_0 + c_1 dn_{BB} + c_2 dn_{BB}^2\right)}$$

$$\frac{\partial L_{ret}^{EV}}{\partial \rho_{RTA}} = -\frac{(L_{HAM} - L_{RTA})}{\rho_{RTA}^2}\left[\frac{(c_0 + c_1 dn_{EV} + c_2 dn_{EV}^2)}{RVS_{EV}(c_0 + c_1 dn_{BB} + c_2 dn_{BB}^2)}(RVS_{SV} - RVS_{BB}) + \frac{(RVS_{SV} - RVS_{EV})}{RVS_{EV}}\right]$$

$$\frac{\partial L_{ret}^{EV}}{\partial dn_{EV}} = \frac{\Delta L_{OBC}}{RVS_{EV}}\frac{c_1 + 2c_2 dn_{EV}}{(c_0 + c_1 dn_{BB} + c_2 dn_{BB}^2)}$$

$$\frac{\partial L_{ret}^{EV}}{\partial dn_{BB}} = \frac{\Delta L_{OBC}}{RVS_{EV}}\frac{(c_1 + 2c_2 dn_{BB})(c_0 + c_1 dn_{EV} + c_2 dn_{EV}^2)}{(c_0 + c_1 dn_{BB} + c_2 dn_{BB}^2)^2}$$

Table 1: Temperature biases [4]

Source	Temperature Bias (K)
BB	0.04
HAM	1.0
RTA	9.0
SH	3.0
CAV	6.0

Table 2: Spectral biases [5]

Band	Spectral Bias (nm)
I4	1.2
I5	4.0
M12	1.2
M13	1.2
M14	4.0
M15	4.0
M16	4.0

Table 3: RVS uncertainties [6]

Band	RVS uncertainty
I4	0.000811
I5	0.000986
M12	0.000818
M13	0.000798
M14	0.001003
M15	0.000875
M16	0.000782

Table 4: Total uncertainties compared to specifications in % of radiance

Band	Scene Temperature					
	190	230	267	270	310	340
I4 spec	--	--	5.0	--	--	--
I4	--	--	2.59	--	--	--
I5 spec	--	--	2.5	--	--	--
I5	--	--	0.46	--	--	--
M12 spec	--	7.0	--	0.7	0.7	0.7
M12	--	8.52	--	0.72	0.38	0.38
M13 spec	--	5.7	--	0.7	0.7	0.7
M13	--	6.82	--	0.69	0.34	0.36
M14 spec	12.3	2.4	--	0.6	0.4	0.5
M14	4.56	0.86	--	0.36	0.29	0.32
M15 spec	2.1	0.6	--	0.4	0.4	0.4
M15	2.30	0.65	--	0.29	0.26	0.30
M16 spec	1.6	0.6	--	0.4	0.4	0.4
M16	2.16	0.58	--	0.29	0.25	0.30

Table 5: Total uncertainties compared to specifications in temperature [K]

Band	Scene Temperature					
	190	230	267	270	310	340
I4 spec	--	--	0.91	--	--	--
I4	--	--	0.48	--	--	--
I5 spec	--	--	1.4	--	--	--
I5	--	--	0.26	--	--	--
M12 spec	--	0.92	--	0.13	0.17	0.21
M12	--	1.06	--	0.13	0.09	0.11
M13 spec	--	0.85	--	0.14	0.19	0.23
M13	--	0.92	--	0.14	0.09	0.12
M14 spec	2.6	0.75	--	0.26	0.23	0.34
M14	0.91	0.27	--	0.15	0.17	0.22
M15 spec	0.56	0.24	--	0.22	0.28	0.34
M15	0.60	0.25	--	0.16	0.18	0.26
M16 spec	0.48	0.26	--	0.24	0.31	0.37
M16	0.61	0.25	--	0.17	0.20	0.28

Figure 1: I4 individual uncertainty terms in EV L_{ret} in % of radiance

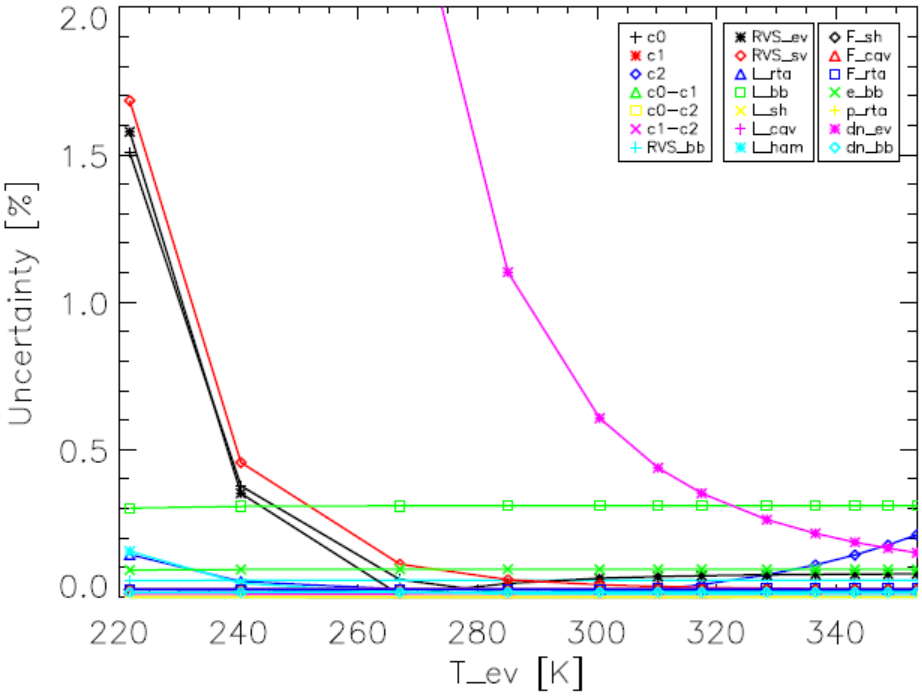

Figure 2: I5 individual uncertainty terms in EV L_{ret} in % of radiance

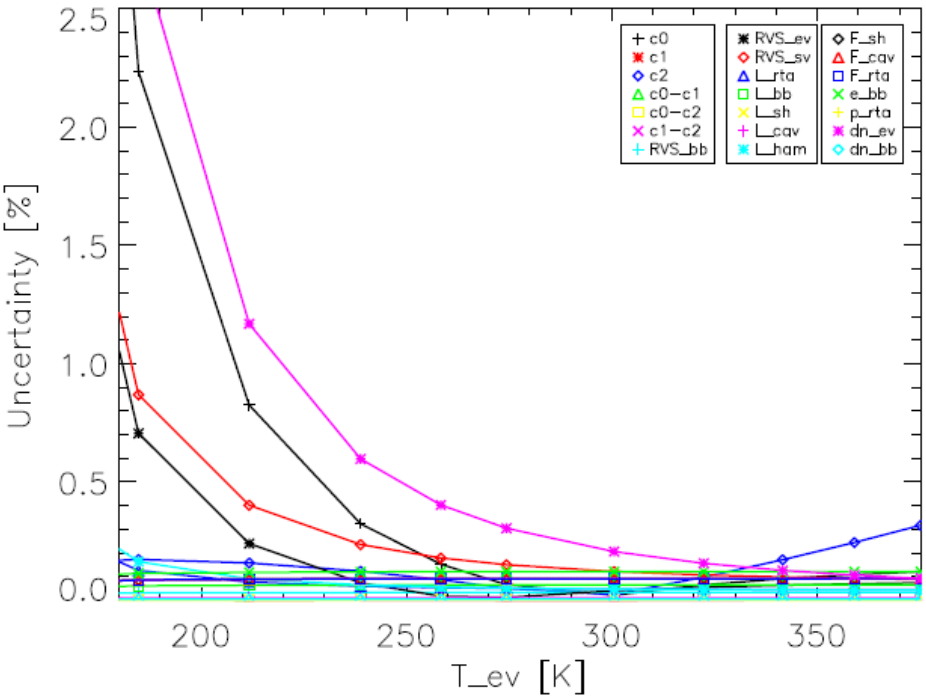

Figure 3: M12 individual uncertainty terms in EV L_{ret} in % of radiance

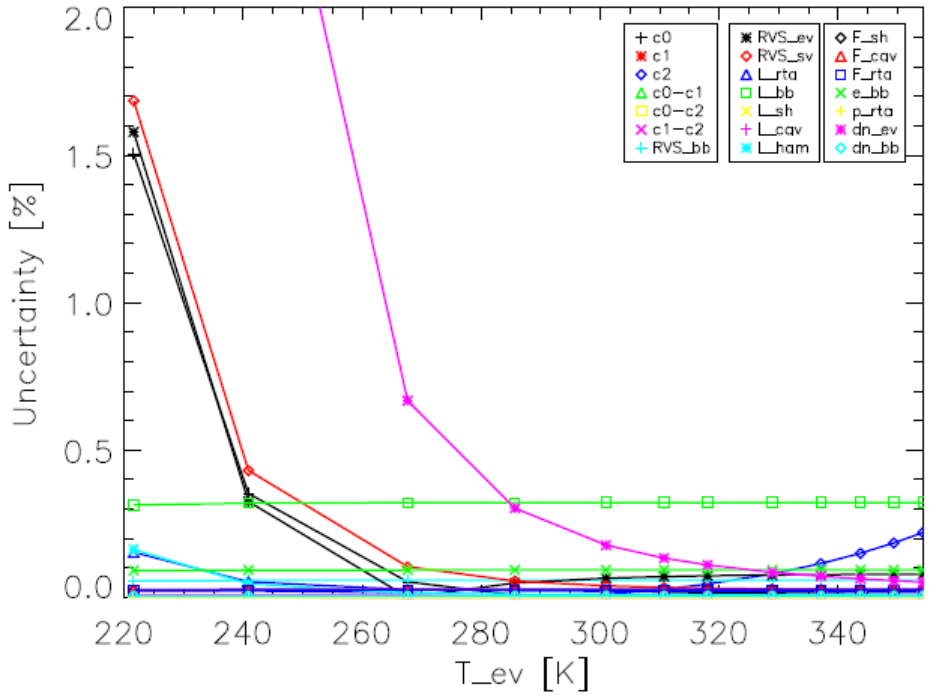

Figure 4: M13 HG individual uncertainty terms in EV L_{ret} in % of radiance

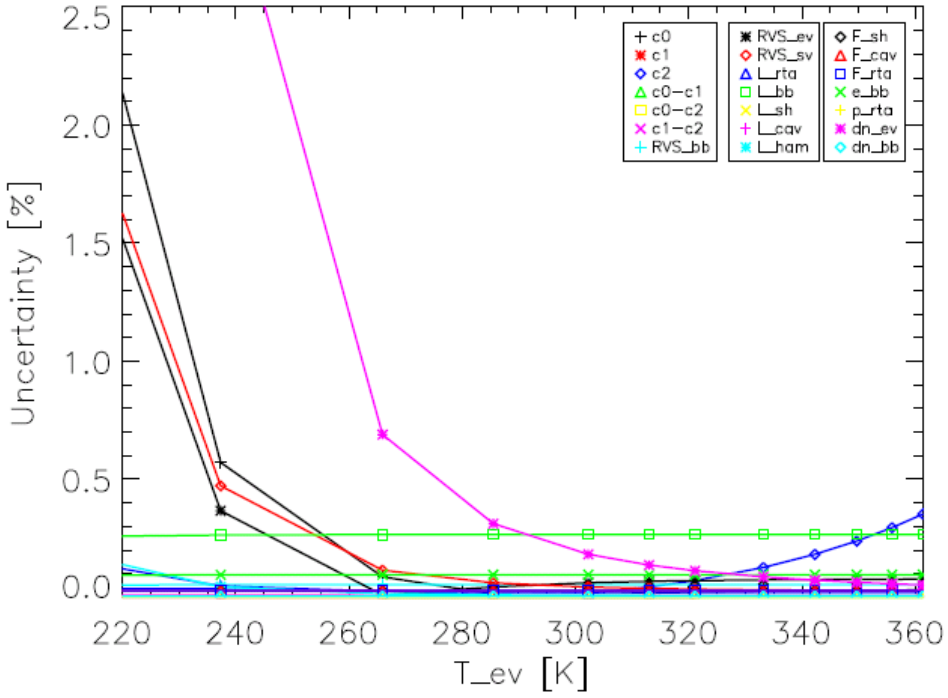

Figure 5: M13 LG individual uncertainty terms in EV L_{ret} in % of radiance

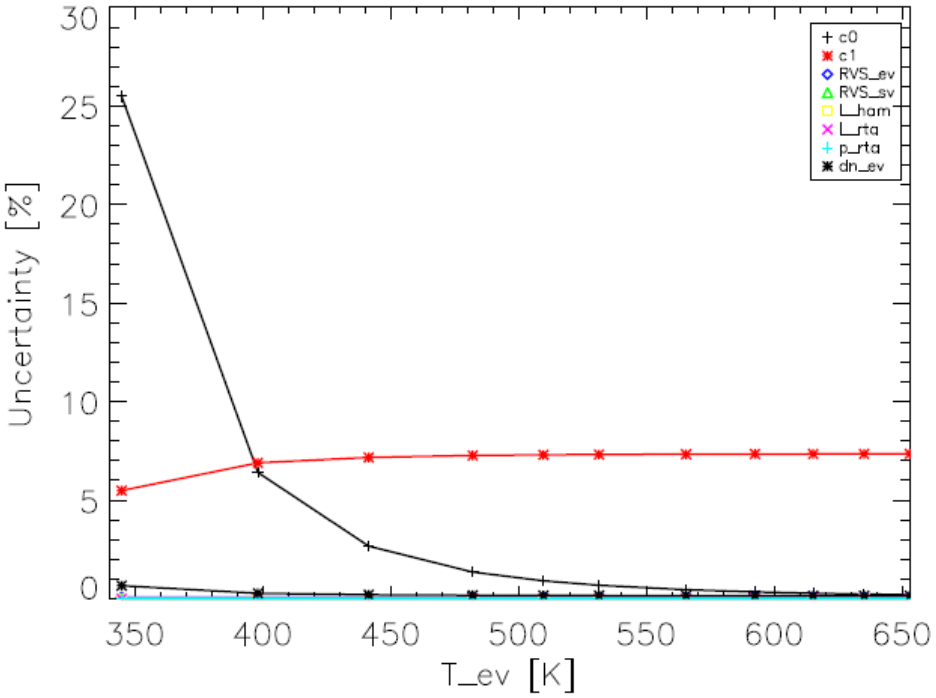

Figure 6: M14 individual uncertainty terms in EV L_{ret} in % of radiance

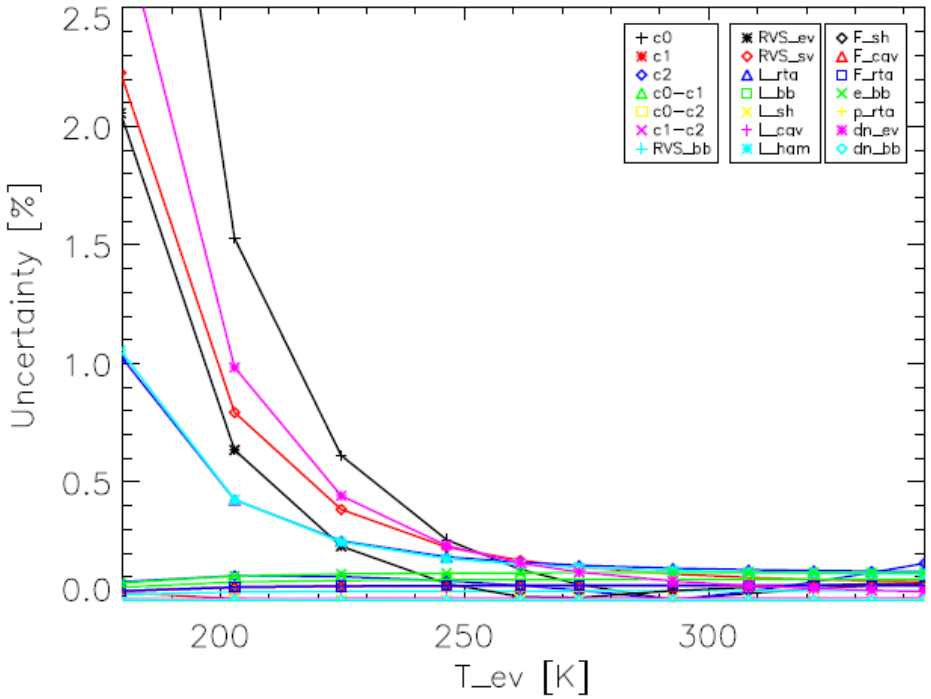

Figure 7: M15 individual uncertainty terms in EV L_{ret} in % of radiance

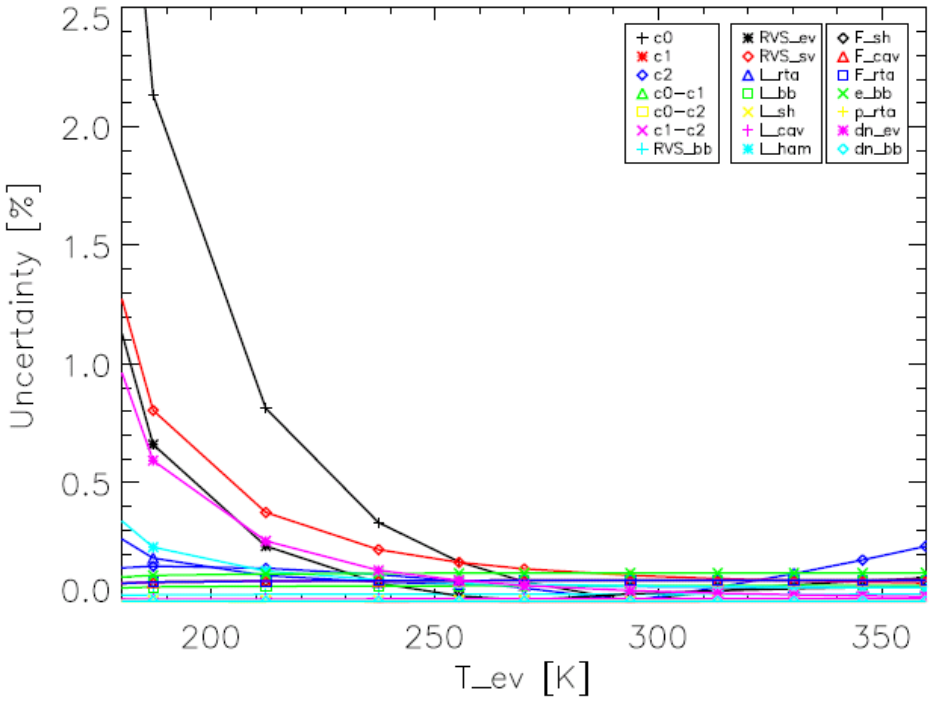

Figure 8: M16 individual uncertainty terms in EV L_{ret} in % of radiance

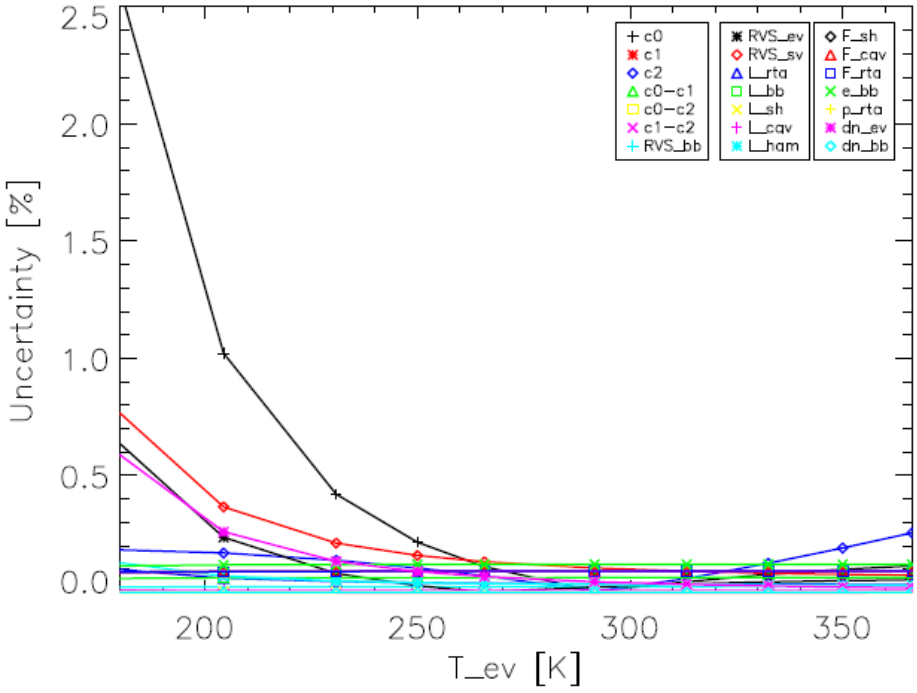

Figure 9: Total uncertainties in EV L_{ret} in % of radiance

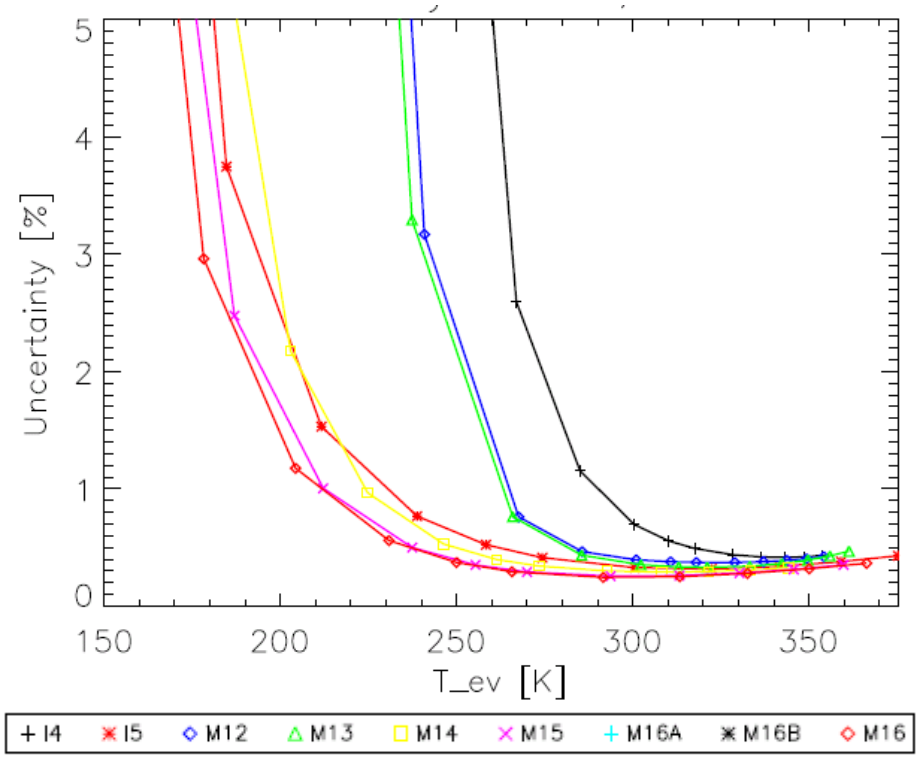

Figure 10: Total uncertainties in EV T_{ret} in temperature [K]

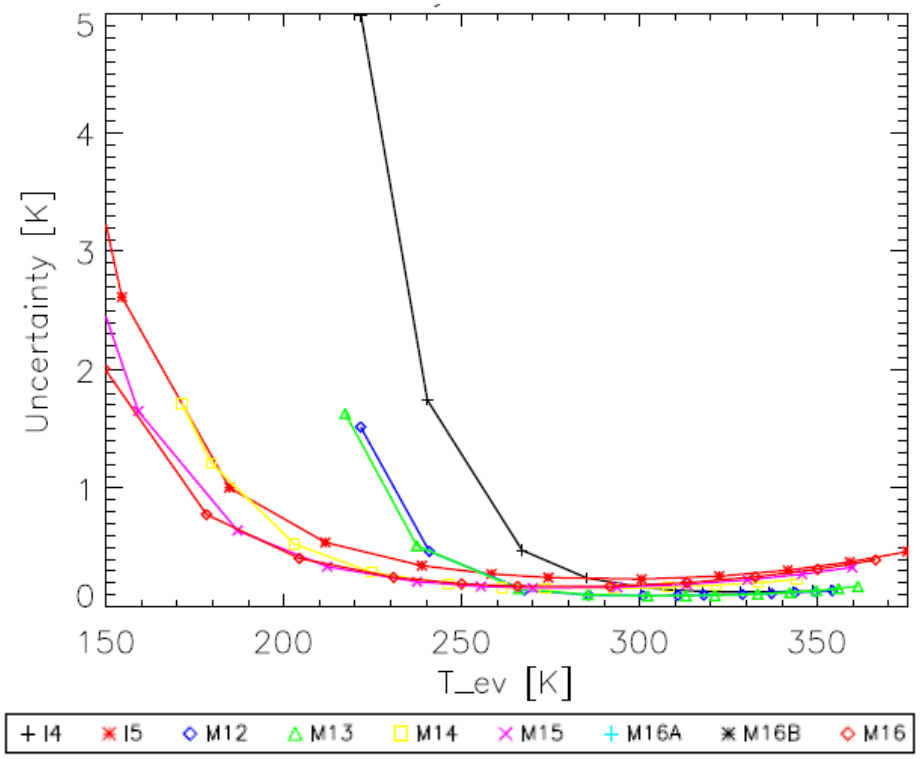

Figure 11: Total uncertainties in M13 LG EV L_{ret} in % of radiance

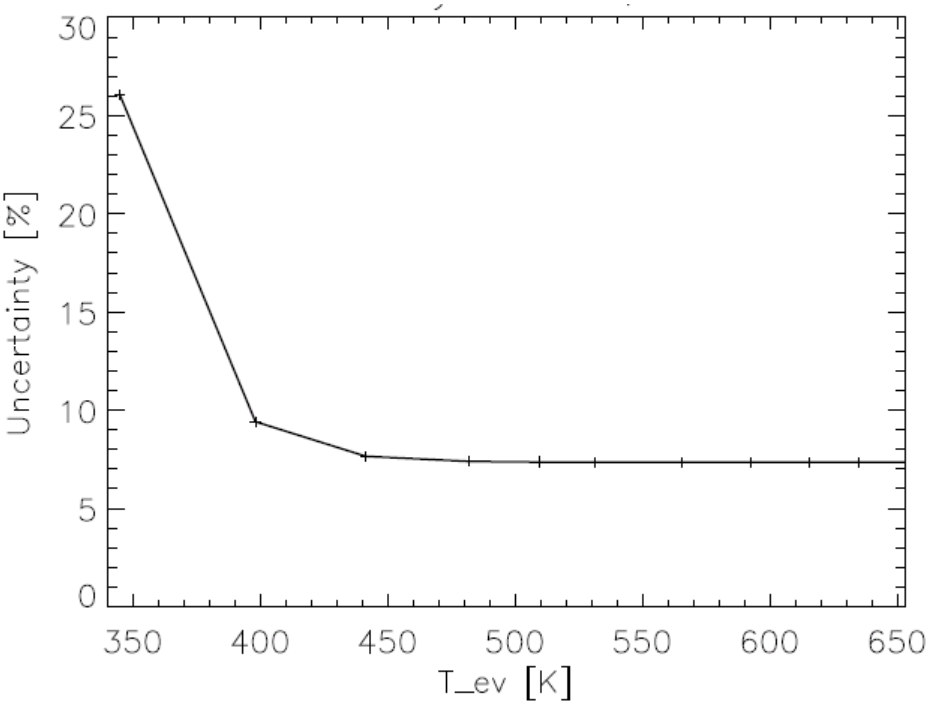

Figure 12: Total uncertainties in M13 LG EV T_{ret} in temperature [K]

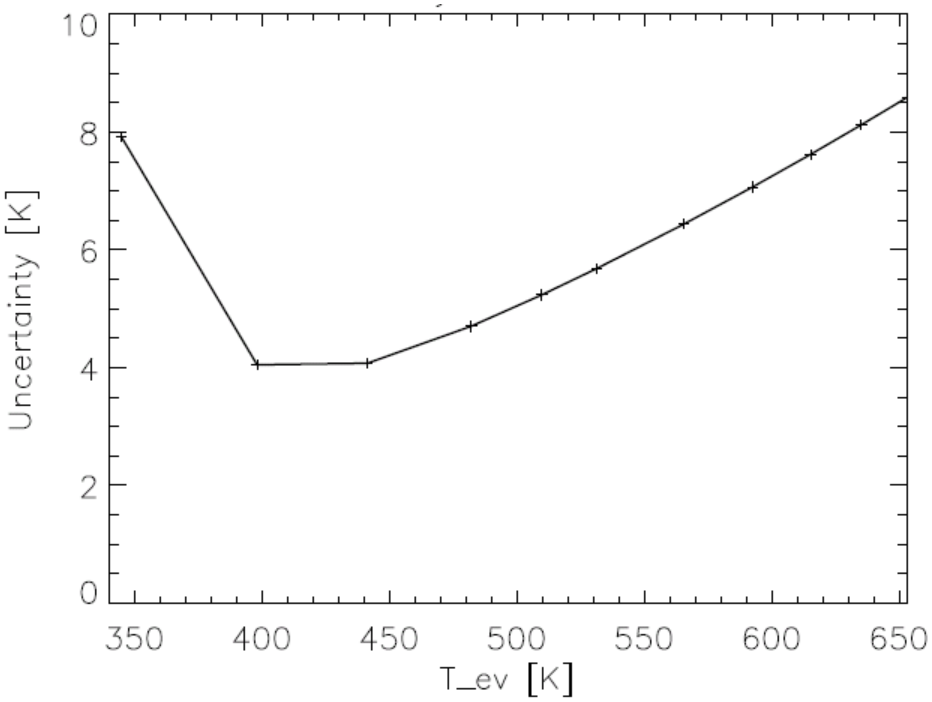

Figure 13: Variation of total uncertainties in I4 EV L_{ret} with scan angle in temperature [K]

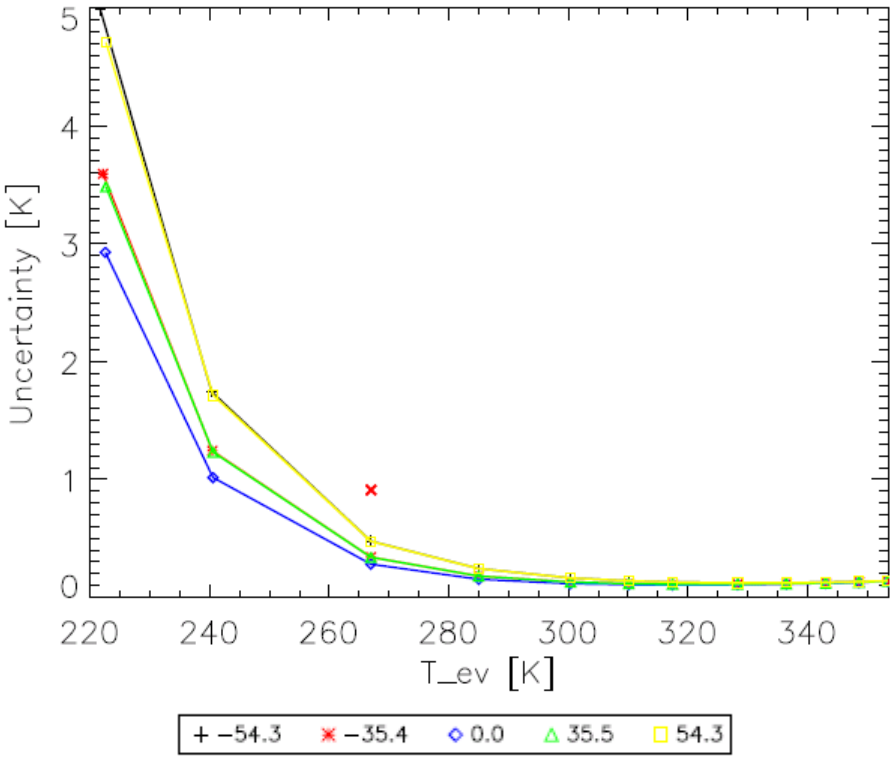

Figure 14: Variation of total uncertainties in I5 EV L_{ret} with scan angle in temperature [K]

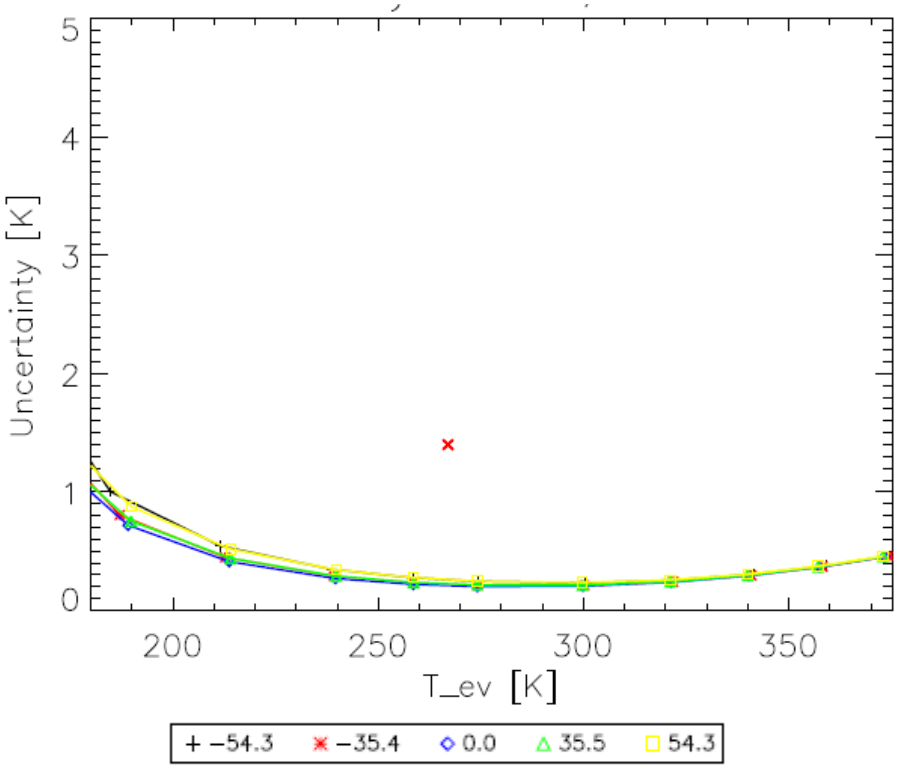

Figure 15: Variation of total uncertainties in M12 EV L_{ret} with scan angle in temperature [K]

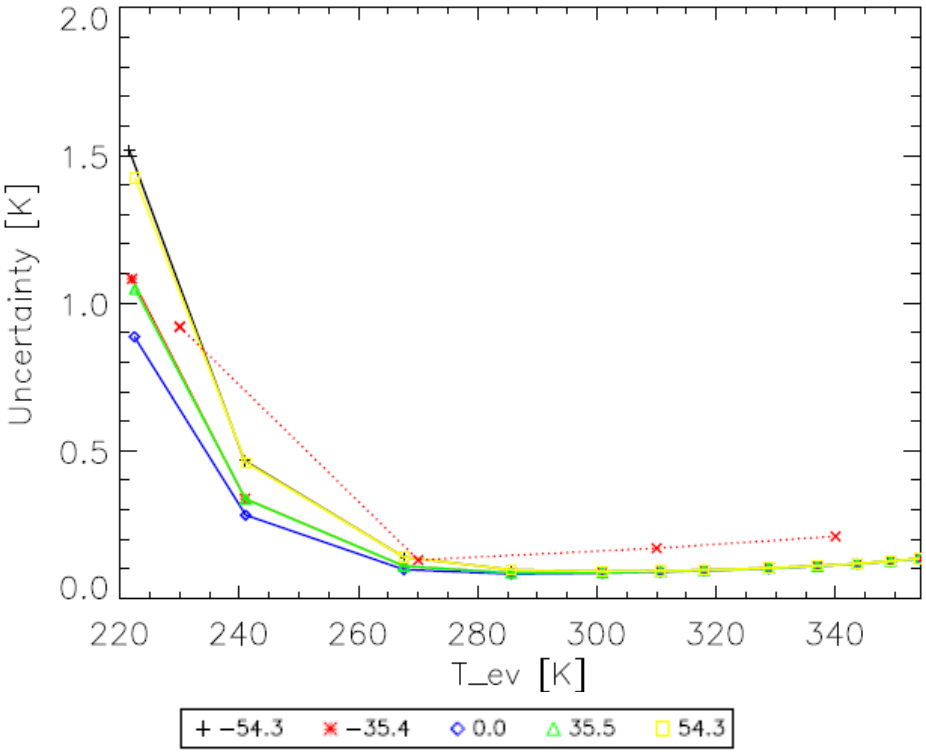

Figure 16: Variation of total uncertainties in M13 HG EV L_{ret} with scan angle in temperature [K]

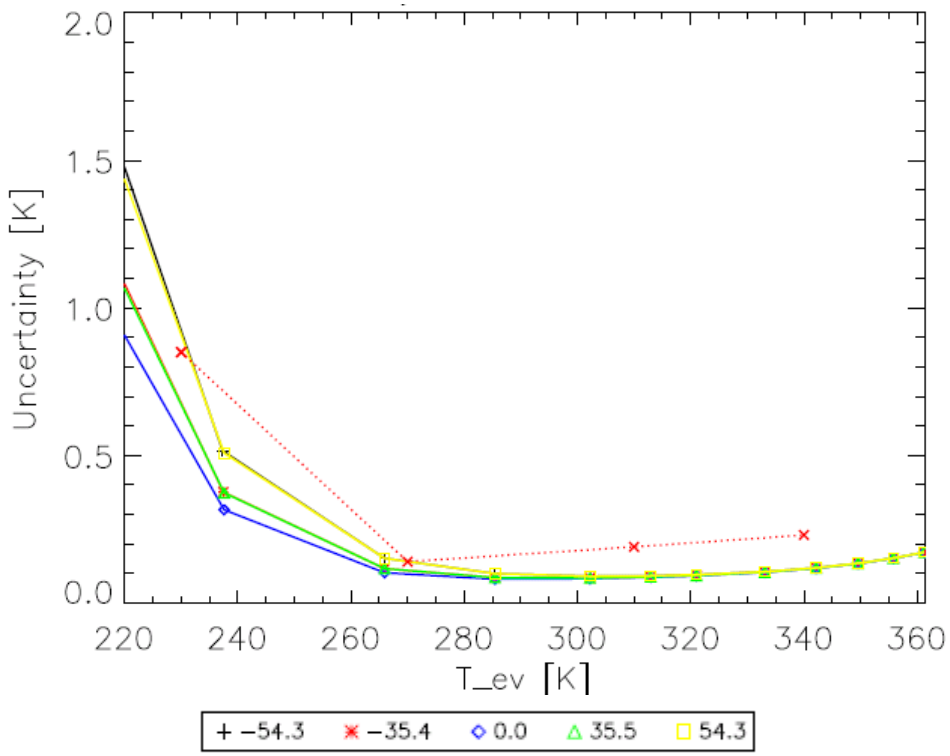

Figure 17: Variation of total uncertainties in M14 EV L_{ret} with scan angle in temperature [K]

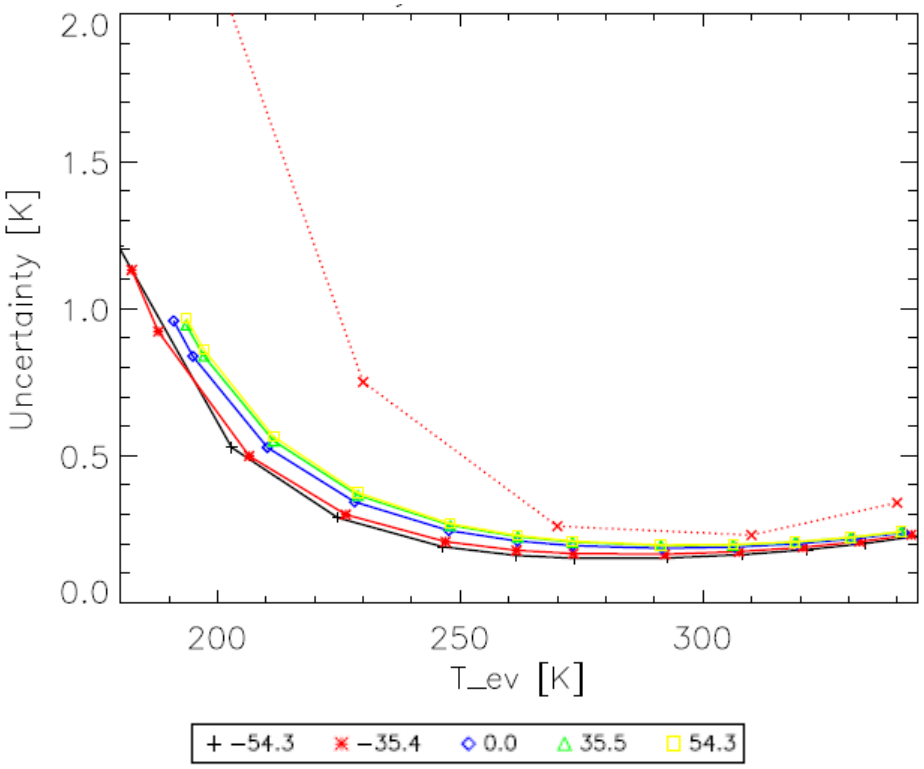

Figure 18: Variation of total uncertainties in M15 EV L_{ret} with scan angle in temperature [K]

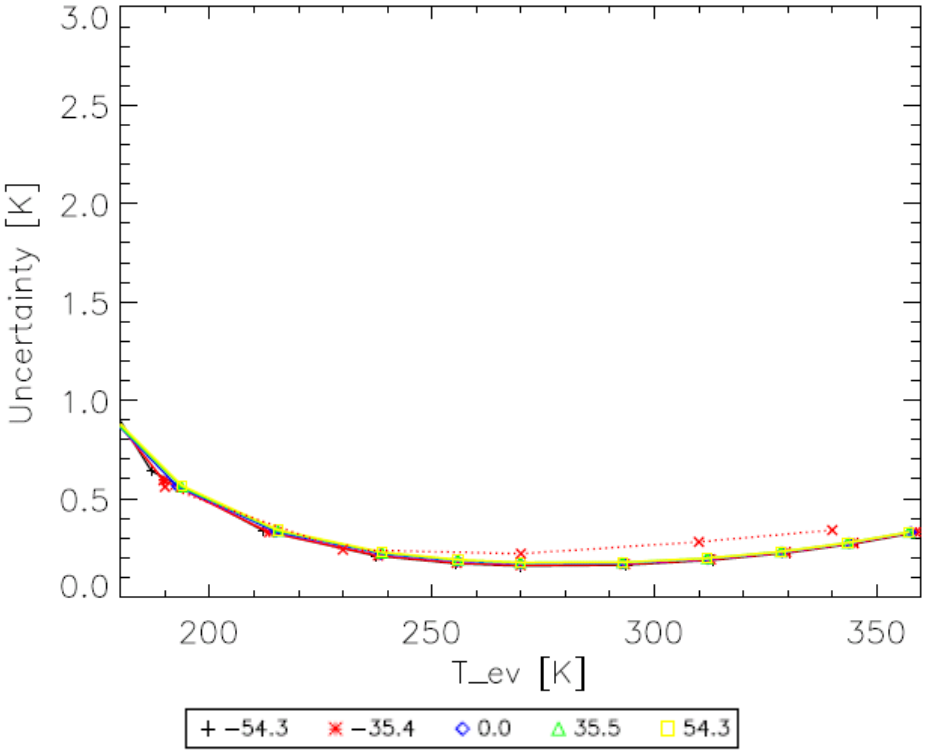

Figure 19: Variation of total uncertainties in M16 EV L_{ret} with scan angle in temperature [K]

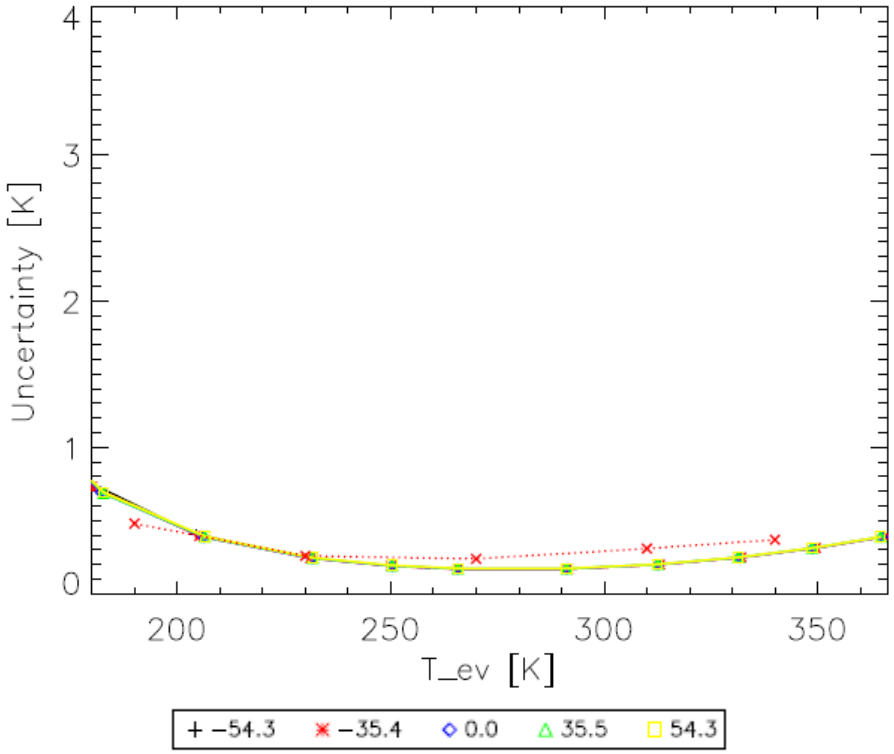

Figure 20: Total uncertainties in EV L_{ret} (baseline and worst-case) in % of radiance

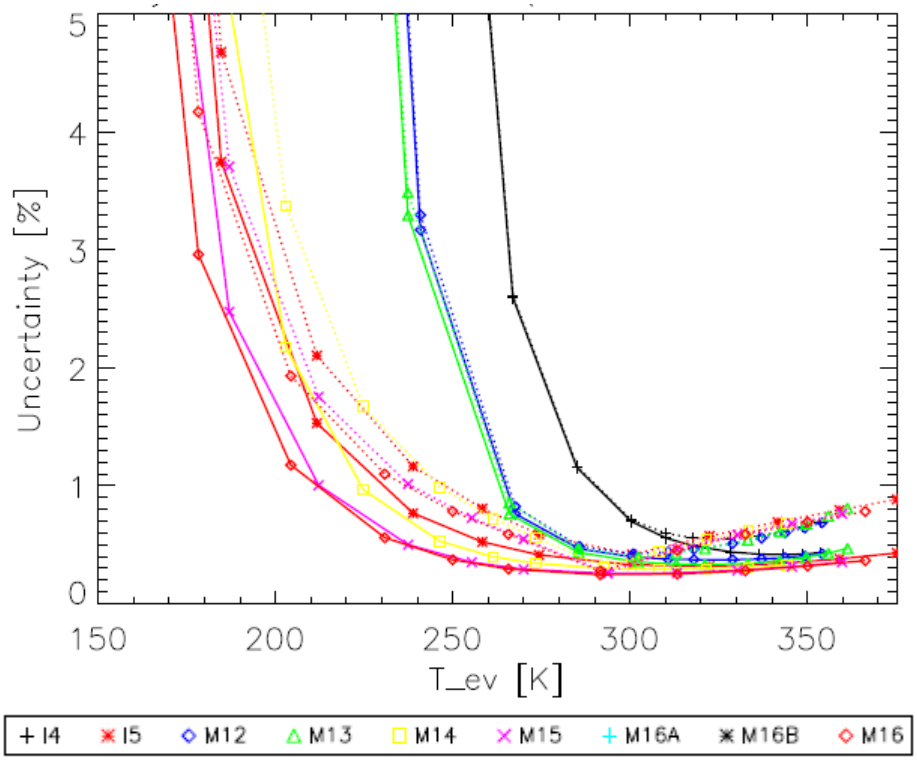

Figure 21: Total uncertainties in EV L_{ret} (baseline and worst-case) in temperature [K]

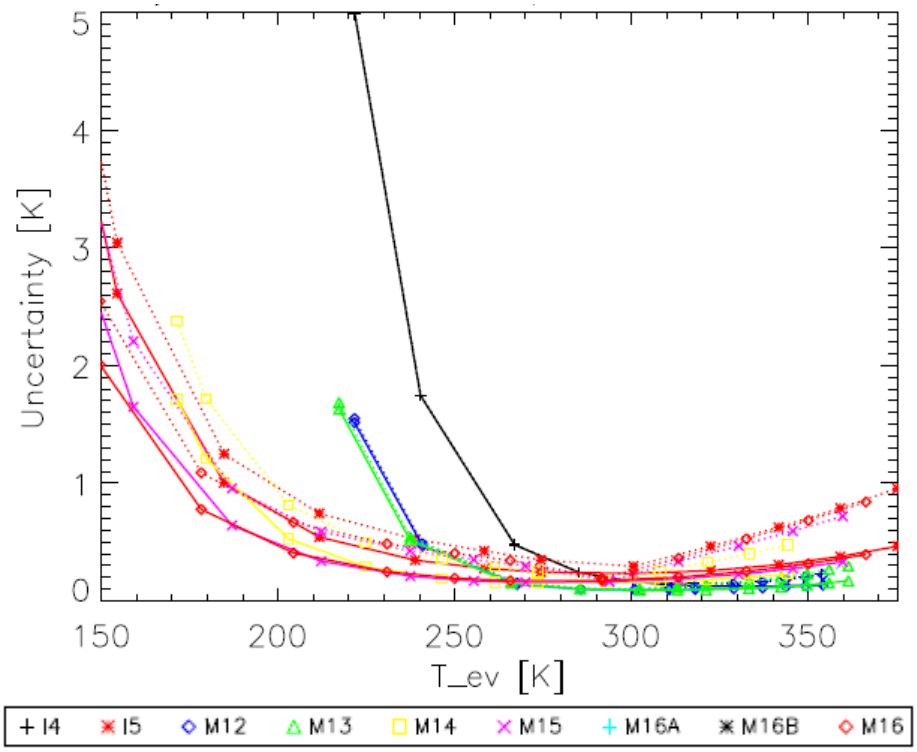
Uncertainty [K]
0
1
2
3
4
5
150
200
250
300
350
T_ev [K]
I4
I5
M12
M13
M14
M15
M16A
M16B
M16